Crystal Structures of Intermediates in the Nitroalkane Oxidase Reaction[†,‡]

Annie Héroux,[§] Dragana M. Bozinovski,[||] Michael P. Valley,[||] Paul F. Fitzpatrick,*[,||,⊥,#] and Allen M. Orville*[,§]

Department of Biology, Brookhaven National Laboratory, Upton, New York 11973, and Departments of Biochemistry and Biophysics and of Chemistry, Texas A&M University, College Station, Texas 77843-2128

Received December 17, 2008; Revised Manuscript Received March 5, 2009

ABSTRACT: The flavoenzyme nitroalkane oxidase is a member of the acyl-CoA dehydrogenase superfamily. Nitroalkane oxidase catalyzes the oxidation of neutral nitroalkanes to nitrite and the corresponding aldehydes or ketones. Crystal structures to 2.2 Å resolution or better of enzyme complexes with bound substrates and of a trapped substrate−flavin adduct are described. The D402N enzyme has no detectable activity with neutral nitroalkanes [Valley, M. P., and Fitzpatrick, P. F. (2003) *J. Am. Chem. Soc. 125*, 8738−8739]. The structure of the D402N enzyme crystallized in the presence of 1-nitrohexane or 1-nitrooctane shows the presence of the substrate in the binding site. The aliphatic chain of the substrate extends into a tunnel leading to the enzyme surface. The oxygens of the substrate nitro group interact both with amino acid residues and with the 2′-hydroxyl of the FAD. When nitroalkane oxidase oxidizes nitroalkanes in the presence of cyanide, an electrophilic flavin imine intermediate can be trapped [Valley, M. P., Tichy, S. E., and Fitzpatrick, P. F. (2005) *J. Am. Chem. Soc. 127*, 2062−2066]. The structure of the enzyme trapped with cyanide during oxidation of 1-nitrohexane shows the presence of the modified flavin. A continuous hydrogen bond network connects the nitrogen of the CN-hexyl-FAD through the FAD 2′-hydroxyl to a chain of water molecules extending to the protein surface. Together, our complementary approaches provide strong evidence that the flavin cofactor is in the appropriate oxidation state and correlates well with the putative intermediate state observed within each of the crystal structures. Consequently, these results provide important structural descriptions of several steps along the nitroalkane oxidase reaction cycle.

Nitroalkane oxidase (NAO)[1] from the soil fungus *Fusarium oxysporum* catalyzes the oxidation of nitroalkanes to the corresponding aldehydes or ketones with the release of nitrite and the consumption of molecular oxygen to yield hydrogen peroxide (*1*). This reaction occurs in distinct reductive and oxidative half-reactions (Scheme 1) (*2, 3*). The reductive half-reaction is initiated by abstraction of the α-proton from the neutral form of the nitroalkane by Asp402, the active site base (*3, 4*). The resulting anion attacks the N5 position of the FAD to form a covalent adduct (*5, 6*); the subsequent elimination of nitrite results in a cationic, electrophilic flavin imine that can be attacked by hydroxide (*7*). Completion of the reductive half-reaction occurs with formation of the aldehyde or ketone product and the reduced FAD. In the oxidative half-reaction, the reduced FAD reacts with molecular oxygen to regenerate the oxidized flavin, producing hydrogen peroxide. This second-order reaction exhibits no detectable intermediates (*3*) and is typical for a flavoprotein oxidase (*8*). Release of product from the oxidized enzyme limits the rate of turnover with primary nitroalkanes, the best substrates (*9*).

NAO is a structural member of the flavoenzyme acyl-CoA dehydrogenase (ACAD) superfamily (*6, 10, 11*). However, NAO does not utilize acyl-CoAs as substrates, nor does ACAD oxidize nitroalkanes (*10*). Indeed, the two types of enzymes appear to bind substrates from opposite orientations, despite the similarity between the thioester-acyl portion of acyl-CoA and the nitro group of nitroalkanes. While the sequences of ACAD family members are only 13−23% identical to that of NAO, the identities are distributed throughout the protein sequence (*1, 6*), and the FAD and active site base are in analogous locations in the active sites of NAO and ACAD (*6*). The initial steps of the catalytic reactions of these enzymes are similar, in that a protein carboxylate abstracts an acidic proton from the substrate (*1, 12*). However, flavin reduction in ACAD occurs by transfer of a hydride from the substrate concerted with or soon after proton

[†] This research was supported in part by grants to P.F.F. from the National Institutes of Health (GM058698) and The Welch Foundation (A-1245) and to A.M.O. from the Offices of Biological and Environmental Research, U.S. Department of Energy, the National Center for Research Resources (2 P41 RR012408) of the National Institutes of Health, and the U.S. Department of Energy. Use of the National Synchrotron Light Source at Brookhaven National Laboratory was supported by the U.S. Department of Energy Office of Basic Energy Sciences, under Contract DE-AC02-98CH10886.

[‡] The atomic coordinates and structure factors have been deposited in the Protein Data Bank (PDB) as entries 3D9D for D402N NAO with 1-nitrohexane, 3D9E for D402N NAO with 1-nitrooctane, 3D9F for S276A NAO with 1-nitrohexane, and 3D9G for wild-type NAO containing the N5-cyanohexyl FAD.

* To whom correspondence should be addressed. A.M.O.: phone, (631) 344-4739; e-mail, amorv@bnl.gov. P.F.F.: phone, (210) 567-8264; fax, (210) 567-8778; e-mail, fitzpatrick@biochem.uthscsa.edu.

[§] Brookhaven National Laboratory.

[||] Department of Biochemistry and Biophysics, Texas A&M University.

[⊥] Department of Chemistry, Texas A&M University.

[#] Current address: Department of Biochemistry, MC 7760, University of Texas Health Science Center at San Antonio, San Antonio, TX 78229-3900.

[1] Abbreviations: NAO, nitroalkane oxidase; ACO, acyl-CoA oxidase; ACAD, acyl-CoA dehydrogenase; K_{ne}, steady-state K_m for nitroethane.

10.1021/bi8023042 CCC: $40.75
Published on Web 03/06/2009

Scheme 1

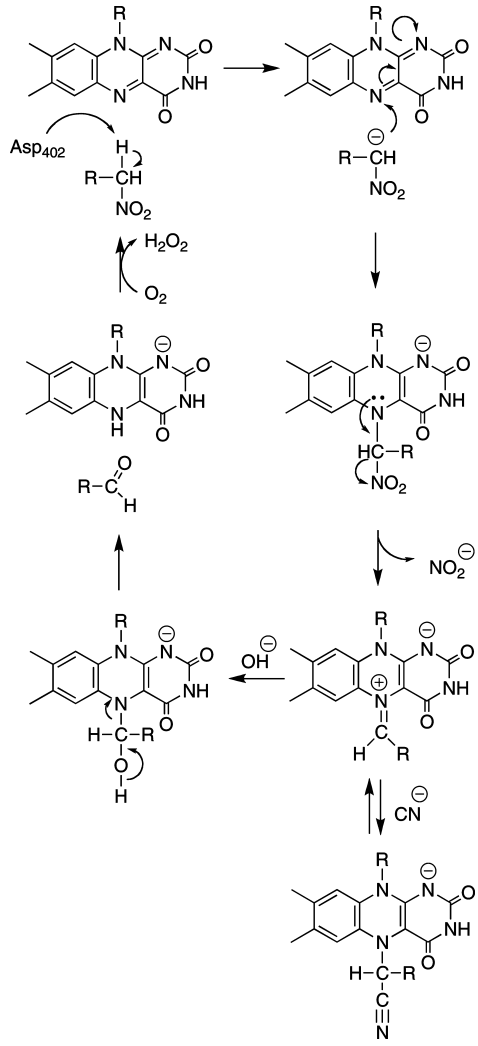

abstraction rather than via attack of the substrate anion on the flavin (*12*). Thus, similar protein environments yield very different outcomes from a similar intermediate in members of the superfamily.

Structural analyses of enzyme−substrate complexes and catalytic intermediates are necessary to explain these differences. Obtaining crystal structures of such intermediates poses significant challenges because of the transient nature of most intermediates and the stability necessary for crystallographic order. In NAO, as in other flavoprotein oxidases, the substrate is rapidly oxidized even in the absence of oxygen; simply adding the substrate to the enzyme will yield the reduced enzyme, from which the products of the reductive half-reaction dissociate. Moreover, substrate binding or proton abstraction is rate-limiting for the reductive half-reaction of NAO (*9*), so that subsequent catalytic intermediates do not accumulate during turnover. Mutagenesis of Asp402 to asparagine or alanine yields an enzyme that will turn over anionic nitroalkane substrates at rates similar to that of the wild-type enzyme reacting with neutral substrates but does not appear to catalyze reactions with the neutral substrate (*4*). Therefore, it was expected that D402N NAO would bind a neutral nitroalkane to form a Michaelis complex but proceed no further in the reaction cycle. Asp402, Arg409, and Ser276 constitute a catalytic triad in NAO (*6, 13*). Kinetic and structural analyses of the effects of mutating Asp402 and Arg409 suggest that both Ser276 and Arg409 are required to position the side chain of Asp402 properly for proton abstraction. We describe here kinetic analyses of the S276A mutant enzyme, confirming the importance of Ser276 in proton abstraction. Since this mutation also greatly decreases the rate of proton abstraction, the S276A enzyme provides another option for obtaining a structure of the Michaelis complex. Further along the catalytic cycle, the cationic flavin imine intermediate does not accumulate; however, it can be trapped with either a nitroalkane anion (*5, 6*) or cyanide (*7*). An N5-cyanoalkyl-FAD is isosteric with the tetrahedral intermediate formed upon attack of hydroxide on the imine intermediate (Scheme 1). We describe here structures of the D402N and S276A enzymes with bound nitroalkane as models for the enzyme−substrate complex in NAO and the structure of NAO trapped with cyanide during turnover as a model for this critical intermediate in the NAO reaction.

EXPERIMENTAL PROCEDURES

Materials. All chemicals were purchased from Sigma-Aldrich Chemical Corp. (Milwaukee, WI), unless otherwise specified. S276A NAO was generated with the QuikChange site-directed mutagenesis kit (Stratagene) as previously described for other NAO mutant proteins (*3*). DNA sequencing of the entire coding sequence of each mutant plasmid was performed at the Laboratory for Plant Genome Technologies of Texas A&M University to confirm the mutation and the lack of undesired mutations. The wild-type and mutant enzymes were expressed in *Escherichia coli* and purified as previously described (*3, 10*). Protein concentrations were determined using an ε_{446} value of 14.2 mM^{-1} cm^{-1}. The cyanide-trapped enzyme was formed by allowing NAO to oxidize 1-nitrohexane in the presence of cyanide as previously described (*7*).

Kinetics. Enzyme activity was measured in air-saturated 100 mM Hepes buffer and 0.1 mM FAD at pH 8.0 and 30 °C by monitoring oxygen consumption with a computer-interfaced Hansatech Clark oxygen electrode (Hansatech Instruments, Pentney King's Lynn, U.K.) as described previously (*13*). To prevent the formation of the substrate anion, stock solutions of nitroethane were prepared in DMSO and assays were initiated by the addition of substrate. Rapid reaction experiments were conducted using an Applied Photophysics SX-20MV stopped-flow spectrophotometer, mixing ~30 μM NAO with 1−100 mM nitroethane, and following the reaction at 455 nm. Enzyme samples were made anaerobic by repeated cycles of vacuum and argon. Glucose oxidase (36 nM) and glucose (5 mM) were added to enzyme solutions to scavenge any residual oxygen. Kinetic data were analyzed using KaleidaGraph (Adelbeck Software, Reading, PA) and Igor Pro (WaveMetrics, Inc., Lake Oswego, OR). Steady-state kinetic parameters were determined by fitting the data to the Michaelis−Menten equation or eq 1

$$v/e = V_{max}S/(K_m + S + S^2/K_i) \quad (1)$$

where K_i is the inhibition constant for substrate inhibition and the other terms have their usual definitions. Steady-state kinetic isotope effects were calculated from eq 2

$$v/e = k_{cat}S/(K_m\{1 + F_i[^D(k_{cat}/K_m) - 1] + S[1 + F_i^D(k_{cat} - 1)]\}) \quad (2)$$

where F_i is the fraction of deuterium in the substrate and $^Dk_{cat}$ and $^D(k_{cat}/K_m)$ are the isotope effects for k_{cat} and k_{cat}/K_m, respectively. Rapid reaction data were fit to eq 3

$$A_t = \Delta A_1 A e^{-k_1 t} + \Delta A_2 e^{-k_2 t} + A_\infty \quad (3)$$

where A_t is the absorbance at 455 nm at time t, ΔA_i is the absorbance change associated with a given phase, k_i is the apparent rate constant for that phase, and A_∞ is the absorbance at infinite time. The rate constants as a function of substrate concentration were fit to eq 4 to produce k_{red}, the limiting first-order rate constant for flavin reduction, and K_d, the apparent dissociation constant.

$$k_{obs} = k_{red}S/(K_d + S + S^2/K_i) \quad (4)$$

Structure Determination. Crystals were obtained using hanging drop vapor-diffusion methods similar to those described previously (*6, 13, 14*), with the exception that spermine was omitted. For the D402N and S276A NAO structures, 1 μL of 1-nitrohexane or 1-nitrooctane was added to a 60 μL stock enzyme solution (~10 mg/mL) immediately prior to setting up the drops. The crystals were grown at 277 K from a mother liquor solution containing 24−30% (w/v) PEG3350, 20% (v/v) glycerol, and 100 mM sodium cacodylate (pH 7.5). In some cases, yellow crystals started appearing within 2 h of setting up the 5 μL hanging drops (1:1 protein/mother liquor mixture). Under similar conditions, colorless crystals of the cyanide-trapped enzyme grew within 2 days; these were harvested immediately since they gradually turned yellow after approximately 1 week. Each crystal was mounted in a nylon loop without further cryoprotection and flash-frozen by quick-submersion in liquid nitrogen. X-ray diffraction data were collected at beamline X12-B, X25, or X29 of the National Synchrotron Light Source with crystals held at 100 K. The data were integrated and scaled with HKL2000 (*15*). The structures were determined by molecular replacement with MolRep from the CCP4 suite of programs (*16*) to resolve the polarity of the trigonal space group. Initially, the search models comprised a homotetramer extracted from the wild-type NAO structure (PDB entry 2c0u) (*6*) from which all solvent and FAD atoms were removed and Asp402 or Ser276 mutated to alanine as appropriate. The solutions indicated that the crystals were in space group $P3_221$ with one α_4 holoenzyme molecule in the asymmetric unit. Model refinement was done with REFMAC 5.2 coupled with COOT (*17*) to mutate residues and assess the refinement cycles. Noncrystallographic symmetry restraints were not applied during the model refinement. Substrate ligands were added in the last stages of model refinement. We also tested several alternative atomic models. For example, atomic models containing several solvent molecules within the electron density for the putative substrate molecules did not refine well. The data collection and model refinement statistics are listed in Table 1. Each structure was confirmed with independent data sets from at least two crystals. Only the highest-quality structure for each is presented here.

Optical Spectra of Single Crystals. Optical absorption spectra were collected from 34 μM wild-type NAO in 500 mM sodium cacodylic acid (pH 7.6) in a 1 cm quartz cuvette with a Perkin-Elmer Lambda 35 spectrometer at room temperature (~23 °C). Single-crystal optical absorption spectra were collected at the Single Crystal μ-Spectroscopy Facility at beamline X26-C of the National Synchrotron Light Source at Brookhaven National Laboratory (*18*). This dedicated facility is available for the general user population. The microspectrophotometer is comprised of components from an XSPECTRA instrument (4DX-ray Systems AB). It can be used for benchtop measurements or aligned with the crystal rotation axes and coincident with the X-ray beam at X26-C. The microscope objectives use parabolic mirrors to achieve 15× magnification and minimize spherical or chromatic aberration. The objectives provide a 24 mm working distance through a 0.4 numerical aperture, which allows for cryocooling and access for other components. The microscope objective was coupled to a 50 μm quartz optical fiber, which yields an incident spot size approximately 25 μm in diameter focused on the cryocooled crystal. The transmitted light was collected from an approximately 75 μm spot size. The incident light (350−850 nm) was from a 75 W Xe research arc lamp (Newport Corp.). An Ocean Optics (Dunedin, FL) USB 4000 spectrophotometer containing a 3648-element Toshiba linear CCD detector was used to collect the optical absorption spectra. The data were processed with SpectraSuite on either a Windows XP or LINUX operating system. The microspectrophotometer was calibrated with a Hg−Ar calibration laser. The reference spectrum in air was collected in the absence of the sample. Typically, optical absorption spectra were obtained by averaging 3−10 spectra, each of which was collected with an integration time between 70 and 200 ms, and with a 3−10-pixel "box car" setting of the CCD detector array. Each crystal was held at 100 K during data collection. We observed that the optical spectra from single crystals are frequently anisotropic and, therefore, collected optical spectra at several crystal angles. The best spectra were usually obtained from needles or plates aligned such that the optical path was normal to the observable flat feature of the particular crystal habit and to the cryoloop. To reduce unusual baseline excursions, no part of the cryoloop intersected the optical spectroscopic axis.

RESULTS

Kinetic Characterization of S276A NAO. To probe the role of the interaction between the hydroxyl group of Ser276 and the carboxylate of the active site base Asp402 in the NAO reaction, Ser276 was changed to alanine by site-directed mutagenesis. The purified recombinant enzyme was characterized using steady-state and rapid-reaction kinetics (Table 2). While the k_{cat}/K_m values are greater for longer chain primary nitroalkanes (*19*), with nitroethane as a substrate the rate-limiting step in substrate oxidation is formation of the nitroethane anion by Asp402 (*9*). Thus, the kinetics with this substrate directly probe cleavage of the substrate C−H bond. Wild-type NAO exhibits substrate inhibition with nitroethane as the substrate, but no substrate inhibition was detected with the S276A enzyme. The k_{cat} and k_{cat}/K_m values for nitroethane are both significantly smaller in the mutant enzyme. Two

Table 1: Crystal Structure Data Collection and Refinement Statistics

	D402N NAO	D402N NAO	S276A NAO	wild-type NAO
PDB entry	3D9D	3D9E	3D9F	3D9G
substrate ligand(s)	1-NO_2-hexane	1-NO_2-octane	1-NO_2-hexane	cyanide with 1-NO_2-hexane
wavelength (Å)	1.1000	1.0809	0.9798	1.0809
space group	$P3_221$	$P3_221$	$P3_221$	$P3_221$
a, *b*, *c* (Å)	107.9, 107.9, 338.4	108.0, 108.0, 338.6	108.3, 108.3, 339.4	109.3, 109.3, 343.9
resolution range (Å)	49−2.10	49−2.20	49−2.20	49−2.15
high-resolution shell (Å)	2.80−2.10	2.28−2.20	2.28−2.20	2.23−2.15
total no. of observations	391271	602598	490262	803662
no. of unique observations	123094	110228	115243	122023
completeness (%)	91.9 (62.1)[a]	93.8 (64.9)	97.4 (83.2)	94.2 (64.9)
redundancy	3.2 (1.6)[a]	5.5 (2.4)	4.3 (4.0)	6.6 (1.8)
R_{sym} (%)[b]	8.9 (44.7)[a]	6.0 (43.4)	6.9 (55.2)	10.4 (28.5)
$I/\sigma I$	13.7 (1.3)[a]	23.2 (1.4)	26.3 (2.2)	27.4 (1.92)
model refinement statistics				
total no. of non-H atoms	14165	13772	13974	14353
no. of residues (protein/ligand/water)	1724/16/650	1723/12/273	1722/16/468	1721/6/840
resolution range (Å)	50−2.1	50−2.2	50−2.2	50−2.15
no. of reflections	116861	104709	109423	115721
R_{cryst} (%)[c]	18.0 (26.7)[a]	19.3 (27.4)[a]	20.2 (27.0)[a]	19.6 (24.3)[a]
R_{free} (%)[d]	21.9 (32.7)[a]	23.3 (33.7)[a]	24.1 (30.5)[a]	23.3 (30.2)[a]
estimated overall coordinate error based on *R* (Å)	0.192	0.232	0.231	0.216
correlation coefficient ($F_o - F_c$)	0.957	0.956	0.955	0.954
Ramachandran statistics				
most favored	1377 (91.5%)	1399 (92.8%)	1377 (91.6%)	1394 (92.6%)
additional allowed	118 (7.8%)	100 (6.6%)	117 (7.7%)	103 (6.8%)
generously allowed	4 (0.3%)	4 (0.3%)	6 (0.4%)	3 (0.2%)
disallowed	6 (0.4%)	4 (0.3%)	4 (0.3%)	5 (0.3%)
average *B* values (Å^2)				
protein	36.07	42.2	44.0	38.0
water	38.8	38.4	43.0	40.8
substrate ligand	50.2	60.2	55.2	−
FAD	29.7	34.4	38.7	32.2
rmsd from ideal geometry				
bond lengths (Å)	0.014	0.011	0.012	0.010
bond angles (deg)	1.53	1.35	1.35	1.30

[a] Highest-resolution shell. [b] $\sum(I_{hkl} - \langle I_{hkl}\rangle)/\sum I_{hkl}$. [c] *R* calculated with the working and the test set inclusive. [d] R_{free} test set calculated with 5% of the data.

Table 2: Kinetic Parameters for Wild-Type and S276A Nitroalkane Oxidase

substrate	kinetic parameter	wild-type NAO	S276A NAO
nitroethane[a]	$k_{cat(nitroethane)}$ (s^{-1})	15 ± 1	1.0 ± 0.01
	$k_{cat}/K_{(nitroethane)}$ (mM^{-1} s^{-1})	6.3 ± 0.4	0.30 ± 0.02
	$K_{(nitroethane)}$ (mM)	2.3 ± 0.2	3.3 ± 0.2
	$K_{i(nitroethane)}$ (mM)	25 ± 3	−
	$^D(k_{cat}/K_m)$	9.2 ± 1.1	9.7 ± 2.0
	$^Dk_{cat(nitroethane)}$	1.4 ± 0.2	2.1 ± 0.4
	k_{red} (s^{-1})	247 ± 5	3.4 ± 0.4
1-nitrohexane	$k_{cat(nitrohexane)}$ (s^{-1})	2.0 ± 0.1	0.30 ± 0.006
	$k_{cat}/K_{(nitrohexane)}$ (mM^{-1} s^{-1})	47 ± 10	1.5 ± 0.2
	$K_{(nitrohexane)}$ (mM)	0.04 ± 0.01	0.20 ± 0.02
	$K_{i(nitrohexane)}$ (mM)	−	130 ± 25
1-nitrooctane	$k_{cat(nitrooctane)}$ (s^{-1})	4.4 ± 0.4	0.2 ± 0.01
	$k_{cat}/K_{(nitrooctane)}$ (mM^{-1} s^{-1})	150 ± 46	1.3 ± 0.2
	$K_{(nitrooctane)}$ (mM)	0.03 ± 0.01	0.3 ± 0.02
	$K_{i(nitrooctane)}$ (mM)	8.3 ± 3.7	26 ± 5

[a] Data for the wild-type enzyme are from ref *3*.

approaches were taken to determine more directly the effect of the mutation on abstraction of the substrate proton. The deuterium kinetic isotope effects on the k_{cat} and k_{cat}/K_m values for nitroethane were determined (Table 2). The $^D(k_{cat}/K_m)$ value is unchanged from the wild-type value. With the wild-type enzyme, the $^D(k_{cat}/K_m)$ value equals the intrinsic isotope effect on the C−H bond cleavage step, reflecting the fact that C−H bond cleavage is fully rate-limiting for flavin reduction. The identical value for the mutant enzyme establishes that C−H bond cleavage is similarly rate-limiting in the reductive half-reaction for the mutant enzyme with nitroethane as the substrate. The $^Dk_{cat}$ value for the wild-type enzyme is close to 1 because product release is substantially slower than the reductive half-reaction and consequently limits the overall turnover (*9*); this isotope effect is increased in the S276A enzyme. Since the k_{cat} value for NAO is simply a combination of the rate constants for flavin reduction and product release (*3*), the k_{cat} and $^Dk_{cat}$ values can be used to calculate the rate constants for these two steps (*13*). The data in Table 2 yield a value of 6.3 ± 1.2 s^{-1} for the rate constant for flavin reduction and a value of 1.2 ± 0.4 s^{-1} for the rate constant for product release. Both values are significantly less than the wild-type values of 247 and 17 s^{-1}, respectively (*3*). As an alternative approach to determining the effect of the S276A mutation on the rate constant for C−H bond cleavage, the rate constant for flavin reduction by nitroethane was determined directly in the stopped-flow spectrophotometer. The decrease in absorbance at 455 nm was composed of two phases comparable in amplitude; only the first phase showed a dependence on the concentration of nitroethane (results not shown). Fitting the apparent first-order rate constants for reduction at different concentrations of nitroethane to eq 4 yielded a value of 3.4 ± 0.4 s^{-1} for the limiting rate constant for flavin reduction, in reasonable agreement with the value calculated from steady-state kinetics. The rate constant for the second phase was the same at all concentrations of nitroethane, with an average value of 0.072 ± 0.017 s^{-1}, and is likely due to dissociation of the product from the reduced enzyme, a step not on the normal catalytic pathway

(*3*). Thus, the mutation decreases the rate constant for removal of the substrate proton by Asp402 by 2 orders of magnitude.

The effects of the S276A mutation on the steady-state kinetics with 1-nitrohexane and 1-nitrooctane are also shown in Table 2. With the wild-type enzyme, these values primarily reflect the rate constants for substrate binding and product release (*3, 9*). Even so, both kinetic parameters decrease significantly for these substrates in the S276A mutant enzyme, with the values for 1-nitrooctane being affected more. While the K_m values for 1-nitrohexane and 1-nitrooctane are increased in the mutant protein, they are still significantly lower than the value for nitroethane.

Overall Description of the Protein Crystals. To obtain structures of mutant enzymes containing a nitroalkane substrate in the active site, 1-nitrohexane or 1-nitrooctane was added to the protein just before the drop was set up. To obtain the cyanide-trapped intermediate, the wild-type enzyme was incubated with 1-nitrohexane in the presence of 1 mM cyanide prior to crystallization. Nitrohexane and nitrooctane were chosen because the enzyme exhibits the largest k_{cat}/K_m values with primary nitroalkanes of four or more carbons as substrates (Table 2) (*19*). This suggests that these tighter-binding substrates should give better occupancy, while the longer aliphatic chain should also better define the binding pocket. High-quality crystals of D402N NAO cocrystallized with nitrohexane or nitrooctane, S276A NAO cocrystallized with nitrohexane, and wild-type NAO trapped with cyanide during turnover with nitrohexane were obtained. The data collection and refinement statistics are collected in Table 1. All of the diffraction data were to 2.2 Å resolution or better, and the structures were determined by molecular replacement with the wild-type enzyme. In all cases, the proteins crystallized in space group $P3_221$, with four subunits in the asymmetric unit, consistent with the tetrameric structure of the wild-type enzyme (*6, 20*). The overall coordinate error for each structure is estimated to be approximately 0.2 Å. Pairwise overlays of the various structures with those of the other mutants or the wild-type enzyme indicated that the rms difference between structures ranges between 0.17 and 0.25 Å. Thus, the overall structure of the enzyme is not perturbed by either mutation, by substrate complex formation, or by formation of the trapped cyanohexyl intermediate.

Single-Crystal Optical Spectra of Enzyme−Substrate Complexes. The greatly reduced catalytic efficiency of the D402N and S276A enzymes makes these mutant enzymes good candidates for crystallization in the presence of neutral nitroalkanes. The substrate should bind near the FAD, but the FAD should remain oxidized in the crystal. The optical spectrum of the enzyme-bound FAD provides a ready measure of its oxidation state; accordingly, visible absorption spectra of the protein while it was in the crystals were obtained. Figure 1[2] shows representative spectra at 100 K of a single crystal of D402N NAO obtained by aerobic cocrystallization with nitrooctane. For the sake of comparison, the optical spectra of oxidized wild-type NAO in two orientations at 100 K, as well as that of oxidized NAO in solution at 295 K, are also shown. The spectrum of the D402N−nitrooctane complex in the crystal is clearly that of the oxidized enzyme. Moreover, the spectra from the single crystals at low temperatures are somewhat better resolved than that of the enzyme in solution, with distinct peaks at 448 and 474 nm, consistent with previous low-temperature spectra of flavoproteins (*21*). Similar spectra were obtained from the D402N and S276A mutant enzymes cocrystallized with nitrohexane (data not shown), establishing that the predominant species in these crystals contain oxidized FAD, despite the presence of saturating concentrations of nitroalkane substrates.

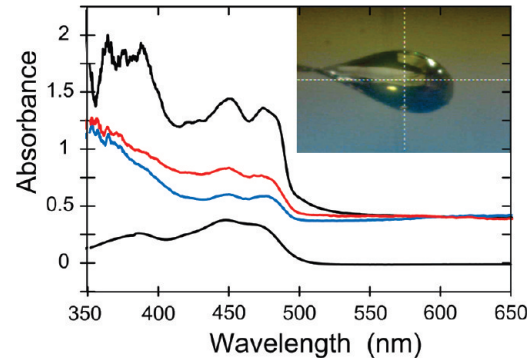

FIGURE 1: Optical absorbance spectra of NAO in solution or from single crystals. The bottom black spectrum is that of 280 μM wild-type NAO in 500 mM cacodylic acid buffer (pH 7.6) at room temperature. The top black spectrum was obtained at 100 K from a single crystal of D402N NAO cocrystallized with 1-nitrooctane. The red and blue spectra in the center are from oxidized wild-type NAO at 100 K obtained from opposite orientations of the cryoloop with respect to the spectroscopic axis. To better facilitate comparisons, the three single-crystal spectra have been normalized for the same absorbance at 600 nm. The oxidized wild-type NAO crystal in the orientation from which the red spectrum was obtained is shown in the inset. In this view, the crystal measures approximately 250 μm in the horizontal direction and 75 μm in the vertical direction. It is approximately in the center of the nylon loop, which measures approximately 235 μm in the vertical direction. The spectroscopic spot size was focused to approximately 25 μm at the intersection of the dashed cross hairs.

In contrast to the crystals of the mutant proteins, those of the wild-type enzyme trapped with cyanide during turnover with 1-nitrohexane were colorless (*7*). Consistent with this observation, the optical spectra of single crystals at 100 K show a single, broad peak with a λ_{max} at approximately 350 nm, and a small fraction of oxidized FAD with shoulders at 448 and 474 nm (data not shown). This is consistent with the presence of the cyanohexyl−flavin adduct as the vast majority species in the crystals (*7*). Over the course of several days at ambient temperature, these crystals turn yellow, indicating formation of the oxidized flavin. The simplest rationale for this observation is that the formation of the cyanohexyl−FAD adduct is reversible. Loss of cyanide from the adduct would re-form the electrophilic imine cation, which could proceed further through catalysis (Scheme 1). This would eventually deplete the 1-nitrohexane, yielding oxidized enzyme.

Crystal Structures of D402N and S276A NAO with Bound Substrates. Figure 2 shows representative electron density maps of the active sites in the aerobic complexes of the mutant enzymes with nitroalkanes. In both the D402N and

[2] The data reported here are for samples that were aligned such that the nylon loop and the flat face of the crystal habit were approximately perpendicular to the optical spectroscopy axis. The optical spectra obtained from single crystal NAO at low temperatures are anisotropic. Consequently, they depend on the rotation angle of the sample with respect to the spectroscopic axis.

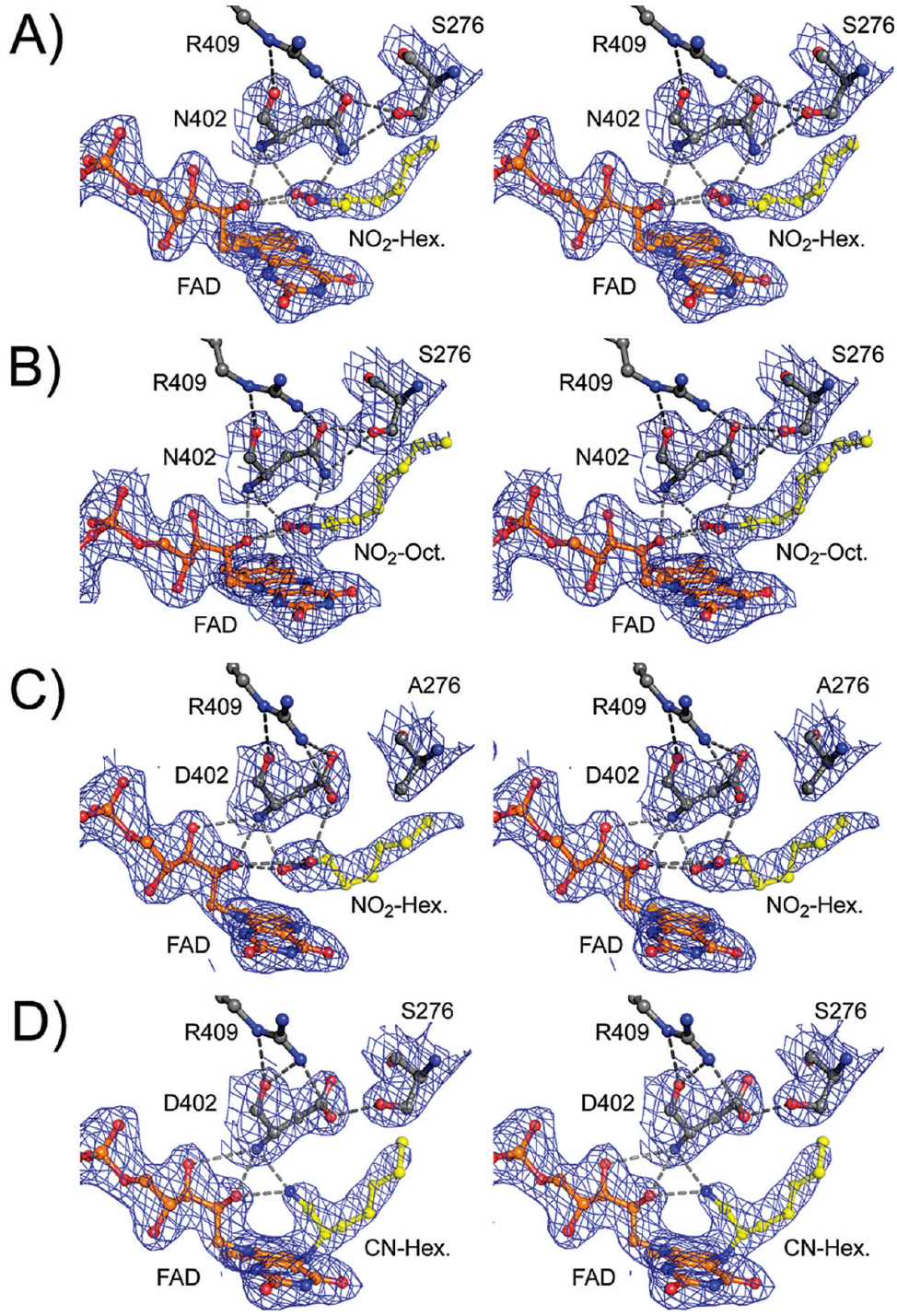

FIGURE 2: Divergent stereo images of the crystal structures of enzyme−substrate complexes and the trapped cyanohexyl−FAD adduct. (A−D) The 4-fold averaged $2F_o - F_c$ electron density maps calculated for the D402N NAO−1-nitrohexane complex (A, 1.5σ), the D402N NAO−1-nitrooctane complex (B, 1.0σ), the S276A NAO−1-nitrohexane complex (C, 1.5σ), and the wild-type NAO−cyanohexyl-FAD complex (D, 1.25σ) are each superimposed on their respective final atomic models. Selected putative hydrogen bonds are shown as gray dashed lines, and the carbon atoms for FAD, the nitroalkane, and the protein are colored orange, yellow, and gray, respectively.

S276A NAO structures, the electron densities for FAD, the active site residues, and an exogenous ligand are all reasonably well resolved. These are all are in comparable positions in the different structures described here (Figure 3), establishing that the mutations do not significantly perturb the active site structure. The electron density observed in each active site is consistent with the particular nitroalkane being present. This supports our conclusion from optical spectroscopy that we have trapped an oxidized enzyme−substrate complex with both mutant proteins. The ability to trap this complex with the S276A enzyme, despite the presence of Asp402, confirms the importance of Ser276 in catalysis.

Figure 4 shows the typical interatomic distances among active site residues, the FAD, and the substrates deduced from the structures described here. We note that each crystal structure exhibits a small degree of variability with respect to the substrate binding orientation within the four independent active sites of each holoenzyme. This variability is consistent with the moderate resolution of the structures

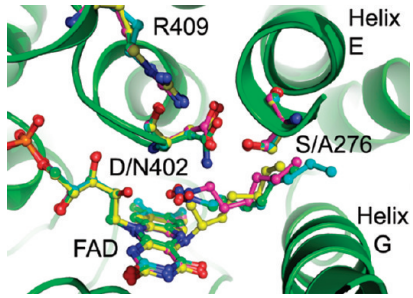

FIGURE 3: Overlay of all four NAO complexes with carbon atoms colored green (D402N NAO with 1-nitrohexane), cyan (D402N NAO with 1-nitrooctane), magenta (S276A NAO with 1-nitrohexane), and yellow (wild-type NAO with cyanohexyl-FAD). The protein backbone for the D402N NAO−1-nitrohexane complex is shown with green ribbons, and in all models, the O, N, and P atoms are colored red, blue, and orange, respectively.

reported here. The position of Arg409 is not significantly altered in any of the mutant structures, with its NH2 group hydrogen-bonded to the backbone carbonyl of the residue at position 402 and the NH1 group interacting with the carboxylate or amide of the side chain at that position. Similarly, the side chain of Ser276 is not affected by the D402N mutation. In contrast, the amide moiety of asparagine in the D402N NAO structures is shifted slightly from the position of the aspartate carboxylate in the wild-type and S276A enzymes, to a position closer to the flavin (Figure 3). The distance from the FAD N5 atom to Asp402 is similar in the wild-type and S276A enzymes (~6.8 Å); it is ~1 Å shorter in the D402N structures (~6.0 Å). The replacement of Asp402 with an asparagine also alters the interaction with Arg409, in that the asparagine side chain is ~0.4 Å closer to the arginine NH2 group in the D402N structures than in S276A or wild-type NAO. While the altered position of Asn402 may indicate that the active site base moves slightly when the substrate is bound, the difference may instead be due to the replacement of a carboxylate with an amide and the resulting weaker interaction with Ser276.

The nitroalkane substrate occupies the same position in the structures of all three mutant proteins (Figure 3), clearly defining the binding mode of the substrate. In the structures of D402N NAO, the α-carbons of both 1-nitrohexane and 1-nitrooctane are 3.4−3.5 Å from the side chain of Asn402, an appropriate placement for proton abstraction. This distance is slightly longer, 3.7 Å, in the S276A enzyme structure. The α-carbon of the nitroalkane is ~3 Å from the flavin N5 position in the D402N enzymes; this distance is increased ~0.5 Å in the S276A enzyme. The two oxygen atoms of the nitro group of the substrates form multiple interactions. In the D402N structures, one substrate oxygen atom is 2.8−2.9 Å from both the amide moiety of Asn402 and the 2′-OH group of the FAD. Both distances are increased significantly in the S276A enzyme, to 3.2 and 3.6 Å, respectively, due to the different position of Asp402 in this structure. The other oxygen atom of the substrate forms one good hydrogen bond (2.8−2.9 Å) with the side chain of the residue at position 402 in all three mutant structures; there is an additional interaction with the 2′-OH group of the FAD which is much stronger (2.7 Å) in the S276A enzyme than in either D402N structure (3.2−3.3 Å). In structures of all the mutant proteins and the wild-type enzyme, the flavin 2′-hydroxyl is ~3.1 Å from a backbone amide nitrogen.

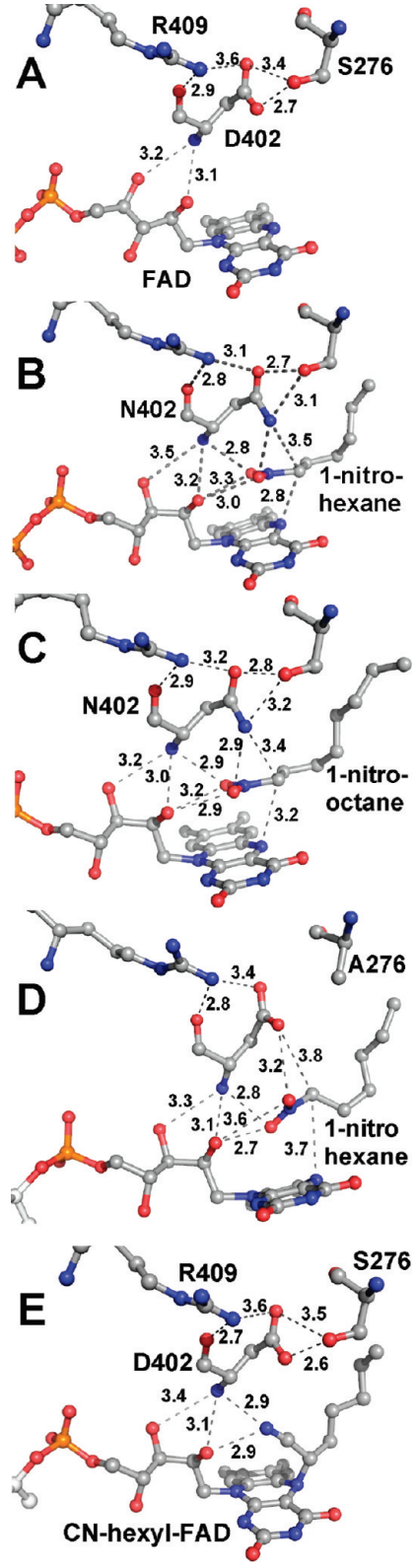

FIGURE 4: Interatomic distances deduced from the structures of (A) wild-type NAO, (B) D402N NAO with 1-nitrohexane, (C) D402N NAO with 1-nitrooctane, (D) S276A NAO with 1-nitrohexane, and (E) wild-type enzyme containing cyanohexyl-FAD.

The substrate alkyl moieties extend away from the flavin into a channel that eventually emerges from the protein surface. In crystals of the wild-type enzyme, this channel contained electron density consistent with a spermine molecule in some of the subunits (*6*). The obvious conclusion drawn from that earlier structure was that this channel is

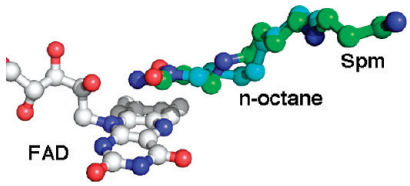

FIGURE 5: Overlay of ligands and FAD in the active sites of wild-type NAO with spermine (Spm, carbon atoms colored green) and D402N NAO with 1-nitrooctane (*n*-octane, carbons colored light blue).

probably the substrate binding site. Spermine was omitted from the crystallization conditions in the structures presented here, and the observed substrate binding orientations confirm this hypothesis. Indeed, the nitroalkanes occupy the same position in the channel as did spermine in the earlier structure (Figure 5), clearly suggesting a substrate access path to the active site. As we reported previously (*6*), the residues surrounding the hexyl and octyl chains are all hydrophobic: Leu80, Ile92, Val95, Ala96, Ala98, Leu99, Leu279, Leu279, Val280, Met283, and Phe401. Thus, the hydrophobicity of this channel complements the aliphatic portion of the substrate ligands and is consistent with the higher k_{cat}/K_M values for longer chain aliphatic substrates. We also note that in crystal structures of the wild-type enzyme and these mutants that are devoid of substrate and spermine, we observe electron density features in the channel of some subunits that can be interpreted as a partially ordered PEG molecule (data not shown).

Crystal Structure of Wild-Type NAO Trapped as the Cyanohexyl Adduct. High-resolution mass spectrometry was previously used to demonstrate formation of a cyanohexyl−FAD adduct during NAO turnover in the presence of cyanide (*7*). The electron density of the active site of the wild-type enzyme trapped by cyanide during turnover with 1-nitrohexane is shown in Figure 2D. There is continuous electron density from the hexyl chain to the flavin N5 atom, confirming the presence of a flavin adduct in these colorless crystals. The electron density for the CN group projects above the *re* face of the adduct; the hexyl side chain occupies the same space as the substrate side chains in the structures of the mutant proteins, with the most significant change being that of the position of the α-carbon (Figure 3). The nitrogen atom of the cyano moiety is within hydrogen bonding distance of the backbone amide of Asp402 and the 2′-hydroxyl of the FAD. It is likely that the hydroxyl group in the tetrahedral intermediate formed during normal turnover is in a position analogous to that of the cyano moiety in the structure presented here. As noted previously for the wild-type enzyme (*6*), there is a second channel from the active site to the enzyme surface on the opposite face from the substrate channel. Although the side chain of Phe273 in NAO causes a constriction of the channel near the FAD, the overall channel is similar to that of the CoA binding site in acyl-CoA dehydrogenase family members. In the structures of NAO described previously and in this structure, this channel contains several water molecules and a glycerol molecule, which was added as a cryoprotectant. In all of the structures reported here, there is a continuous hydrogen bond network of solvent molecules and glycerol from the FAD 2′-hydroxyl to the protein surface (Figure 6).

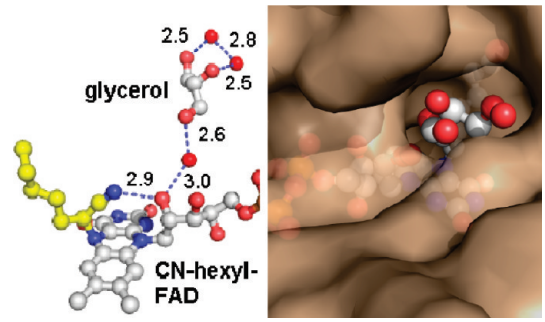

FIGURE 6: Channel of water molecules from the active site to the surface from the cyanohexyl−FAD structure: left, deduced hydrogen bonding interactions, with the carbon atoms from the hexyl moiety colored yellow; right, surface rendering to illustrate the channel. The orientation of this view is rotated approximately 180° relative to all other figures. The view of the surface rendering is from the exterior toward the glycerol molecule.

DISCUSSION

The role of Asp402 as the active site base in NAO was previously established by site-directed mutagenesis (*3, 4*). Critically, the D402N enzyme is essentially inactive with neutral nitroalkanes but has nearly wild-type activity when the substrate carbanion is used. In the active site of NAO, Asp402 interacts with two other residues, Arg409 and Ser276. The importance of Arg409 for abstraction of a proton from the substrate by Asp402 has been confirmed by site-directed mutagenesis (*13*). The rate constant for C−H bond cleavage by the R409K enzyme is only 1% of the wild-type value. Direct structure determination of the mutant protein established that this can be explained by the side chain of the lysyl residue being too short to interact with the carboxylate of the aspartate, altering the position of the active site base. The characterization of the S276A enzyme described here establishes that this residue is also important for proton abstraction by Asp402, in that the rate constant for removal of the substrate proton is also ~100-fold smaller for the mutant protein than the wild-type value. The structure of the mutant protein described here establishes that this mutation does not perturb the active site structure, so that the deleterious effect of the mutation on catalysis can be ascribed to the loss of the hydrogen bond between Asp402 and Ser276.

This work also demonstrates that the lack of activity of the D402N enzyme and the decreased activity of the S276A enzyme both provide access to models for the enzyme−substrate complex. The hydrophobic chain of the substrate extends into a hydrophobic channel that continues to the surface of the protein, suggesting a substrate access route to the active site. The nitro group of the substrate is held in place by interactions with both amino acid residues and the 2′-hydroxyl of the FAD. The hydrogen bonds deduced among the substrate oxygen atom(s), the FAD 2′-hydroxyl, and the backbone amide of Asp(Asn)402 in our structures resemble those seen in the structures of medium chain ACAD in complex with either substrates (PDB entry 1mde) (*11, 22*) or a transition-state analogue (PDB entry 1udy) (*23*). In that enzyme, the carbonyl of the acyl-CoA substrate forms hydrogen bonds with the flavin 2′-hydroxyl and the backbone amide of Glu376, the active site base (Figure 7). Replacement of the FAD with 2′-deoxy-FAD decreases the activity by 10^7-fold (*24*), clearly demonstrating the importance of this

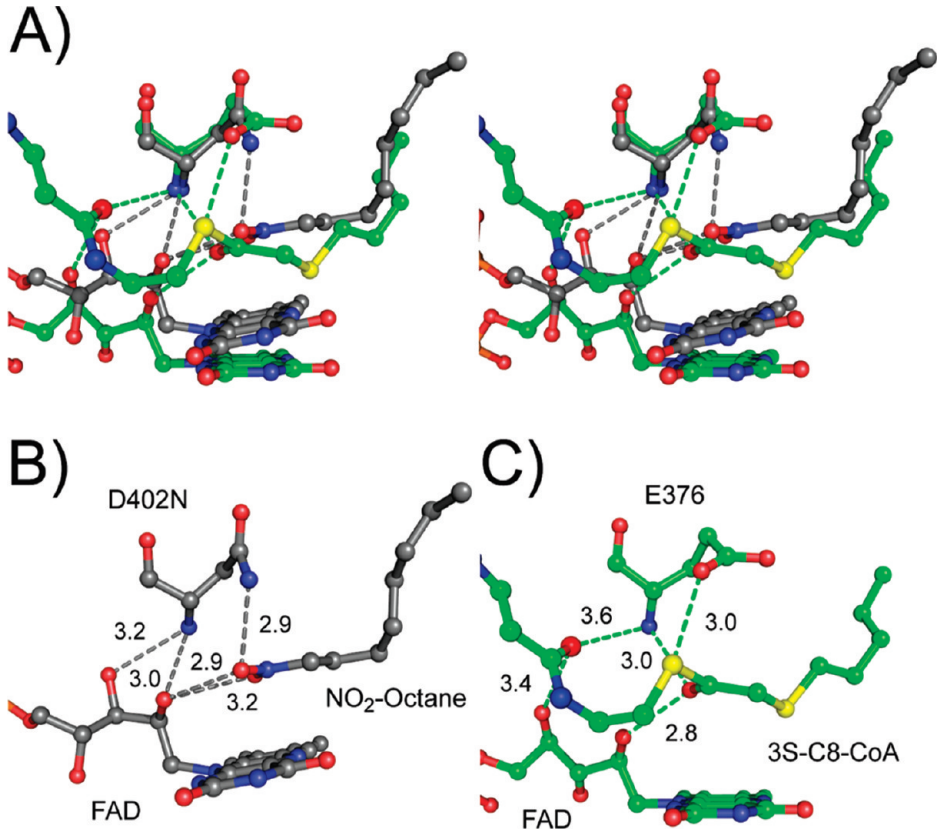

FIGURE 7: Overlay of the D402N NAO−NO_2-octane complex with the medium chain ACAD−3-thiaoctanoyl-CoA (3S-C8-CoA) complex. (A) The divergent stereo overlay is shown with C atoms and dashed lines indicating potential hydrogen bonds colored gray and green for the NAO and ACAD (PDB entry 1udy) structures, respectively. The N, O, and S atoms are colored blue, red, and yellow, respectively. (B) The same orientations and color schemes with distances labeled are shown for the NAO (B) and ACAD (C) structures.

interaction in that enzyme. The presence of these interactions in both NAO and ACAD demonstrates that the conservation of the catalytic apparatus for proton abstraction in this family extends beyond the location of the active site base and the FAD.

The α-carbons of 1-nitrohexane and 1-nitrooctane are well-positioned for abstraction of a proton by Asp402 and subsequent attack of the resulting carbanion on the flavin N5 atom. The relative positions of Asp402, the substrate, and the flavin make it unlikely that proton abstraction and addition to the flavin are concerted. Since Asp402 is on the opposite side of the substrate from the flavin, the resulting carbanion must rehybridize before nucleophilic addition to the flavin can occur. The altered position of the N402 amide in the D402N mutant structures compared to that of the Asp402 suggests that this rehybridization may be accompanied by movement of the carboxylate.

The flavin adduct formed by trapping the enzyme with cyanide during turnover with 1-nitrohexane is an excellent model for the intermediate formed during catalysis by attack of hydroxide on the electrophilic imine cation. The position of the cyano moiety suggests that it accesses the flavin via the water/glycerol-filled channel on the opposite side of the active site from the substrate channel. It is likely that the presence of the alkyl chain for 1-nitrohexane precludes access by the latter path. We have previously described the structure of a nitrobutyl−flavin adduct formed during turnover of nitroethane in the presence of nitroethane anion (*6*). Figure 8 shows an overlay of the two flavin adducts. The structure of the nitrobutyl−FAD adduct is consistent with the nitroethane anion attacking the electrophilic intermediate by entering through the substrate channel due to the inability of the short ethyl chain to block the channel. Consistent with the entry of nitroalkane anions through the substrate channel, nitroalkanes longer than nitroethane form such anion-derived adducts much more slowly.[3] The water/glycerol channel is also the likely source of the hydroxide that attacks the imine intermediate during the normal catalytic reaction. In this region of the protein, there is no obvious amino acid residue which could act as a base to accept a proton from water to form hydroxide. A reasonable hypothesis is that the 2′-hydroxyl of the FAD is the base. The proton could be shuttled to the exterior of the protein through the series of hydrogen-bonded water molecules. The 2′-hydroxyl of the

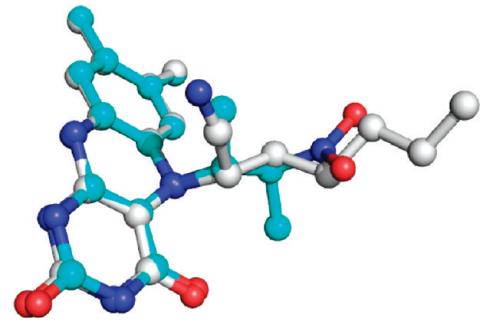

FIGURE 8: Overlay of NAO flavin adducts formed during turnover of nitrohexane in the presence of cyanide (light gray carbon atoms) and from a mixture of neutral and anionic nitroethane (light blue carbon atoms) (PDB entry 2cou).

[3] G. Gadda and P. F. Fitzpatrick, unpublished observations.

FAD thus plays multiple roles in the NAO reaction. It binds the nitro moiety of the substrate in the initial enzyme−substrate complex; once nitrite has been lost, the hydroxyl can act as a base to complete the reaction.

REFERENCES

1. Fitzpatrick, P. F., Orville, A. M., Nagpal, A., and Valley, M. P. (2005) Nitroalkane oxidase, a carbanion-forming flavoprotein homologous to Acyl-CoA dehydrogenase. *Arch. Bicohem. Biophys. 433*, 157–165.
2. Heasley, C. J., and Fitzpatrick, P. F. (1996) Kinetic mechanism and substrate specificity of nitroalkane oxidase. *Biochem. Biophys. Res. Commun. 225*, 6–10.
3. Valley, M. P., and Fitzpatrick, P. F. (2003) Reductive half-reaction of nitroalkane oxidase: Effect of mutation of the active site aspartate to glutamate. *Biochemistry 42*, 5850–8566.
4. Valley, M. P., and Fitzpatrick, P. F. (2003) Inactivation of nitroalkane oxidase upon mutation of the active site base and rescue with a deprotonated substrate. *J. Am. Chem. Soc. 125*, 8738–8739.
5. Gadda, G., Edmondson, R. D., Russel, D. H., and Fitzpatrick, P. F. (1997) Identification of the naturally occurring flavin of nitroalkane oxidase from *Fusarium oxysporum* as a 5-nitrobutyl-FAD and conversion of the enzyme to the active FAD-containing form. *J. Biol. Chem. 272*, 5563–5570.
6. Nagpal, A., Valley, M. P., Fitzpatrick, P. F., and Orville, A. M. (2006) Crystal structures of nitroalkane oxidase: Insights into the reaction mechanism from a covalent complex of the flavoenzyme trapped during turnover. *Biochemistry 45*, 1138–1150.
7. Valley, M. P., Tichy, S. E., and Fitzpatrick, P. F. (2005) Establishing the kinetic competency of the cationic imine intermediate in nitroalkane oxidase. *J. Am. Chem. Soc. 127*, 2062–2066.
8. Massey, V. (1994) Activation of molecular oxygen by flavins and flavoproteins. *J. Biol. Chem. 269*, 22459–22462.
9. Gadda, G., Choe, D. Y., and Fitzpatrick, P. F. (2000) Use of pH and kinetic isotope effects to dissect the effects of substrate size on binding and catalysis by nitroalkane oxidase. *Arch. Bicohem. Biophys. 382*, 138–144.
10. Daubner, S. C., Gadda, G., Valley, M. P., and Fitzpatrick, P. F. (2002) Cloning of nitroalkane oxidase from *Fusarium oxysporum* identifies a new member of the acyl-CoA dehydrogenase superfamily. *Proc. Natl. Acad. Sci. U.S.A. 99*, 2702–2707.
11. Kim, J. J., and Miura, R. (2004) Acyl-CoA dehydrogenases and acyl-CoA oxidases. Structural basis for mechanistic similarities and differences. *Eur. J. Biochem. 271*, 483–493.
12. Ghisla, S., and Thorpe, C. (2004) Acyl-CoA dehydrogenases. A mechanistic overview. *Eur. J. Biochem. 271*, 494–508.
13. Fitzpatrick, P. F., Valley, M. P., Bozinovski, D. M., Shaw, P. G., Héroux, A., and Orville, A. M. (2007) Mechanistic and Structural Analyses of the Roles of Arg409 and Asp402 in the Reaction of the Flavoprotein Nitroalkane Oxidase. *Biochemistry 46*, 13800–13808.
14. Nagpal, A., Valley, M. P., Fitzpatrick, P. F., and Orville, A. M. (2004) Crystallization and preliminary analysis of active nitroalkane oxidase in three crystal forms. *Acta Crystallogr. D60*, 1456–1460.
15. Otwinowski, Z., and Minor, W. (1997) Processing of X-ray diffraction data collected in oscillation mode. *Methods Enzymol. 276*, 307–326.
16. Collaborative Computational Project No. 4 (1994) The CCP4 suite: Programs for protein crystallography. *Acta Crystallogr. D50*, 760–763.
17. Emsley, P., and Cowtan, K. (2004) Coot: Model-building tools for molecular graphics. *Acta Crystallogr. D60*, 2126–2132.
18. Orville, A. M., Lountos, G. T., Finnegan, S., Gadda, G., and Prabhakar, R. (2009) Crystallographic, spectroscopic, and computational analysis of a flavin C4a-oxygen adduct in choline oxidase. *Biochemistry 48*, 720–728.
19. Gadda, G., and Fitzpatrick, P. F. (1999) Substrate specificity of a nitroalkane oxidizing enzyme. *Arch. Bicohem. Biophys. 363*, 309–313.
20. Gadda, G., and Fitzpatrick, P. F. (1998) Biochemical and physical characterization of the active FAD-containing form of nitroalkane oxidase from *Fusarium oxysporum*. *Biochemistry 37*, 6154–6164.
21. Siddiqui, M. S. U., and Stanley, R. J. (2005) A cryogenic optical waveguide spectrometer for the measurement of low-temperature absorption spectra of dilute biological samples. *Anal. Biochem. 337*, 121–129.
22. Kim, J.-J. P., Wang, M., and Paschke, R. (1993) Crystal structures of medium-chain acyl-CoA dehydrogenase from pig liver mitochondria with and without substrate. *Proc. Natl. Acad. Sci. U.S.A. 90*, 7523–7527.
23. Satoh, A., Nakajima, Y., Miyahara, I., Hirotsu, K., Tanaka, T., Nishina, Y., Shiga, K., Tamaoki, H., Setoyama, C., and Miura, R. (2003) Structure of the transition state analog of medium-chain acyl-CoA dehydrogenase. Crystallographic and molecular orbital studies on the charge-transfer complex of medium-chain acyl-CoA dehydrogenase with 3-thiaoctanoyl-CoA. *J. Biochem. (Tokyo, Jpn.) 134*, 297–304.
24. Engst, S., Vock, P., Wang, M., Kim, J.-J. P., and Ghisla, S. (1999) Mechanism of activation of acyl-CoA substrates by medium chain acyl-CoA dehydrogenase: Interaction of the thioester carbonyl with the flavin adenine dinucleotide ribityl side chain. *Biochemistry 38*, 257–267.

BI8023042